Eur. J. Mineral.
2006, **18**, 463-469

Crystal chemistry of the halotrichite group $X Al_2(SO_4)_4 \cdot 22H_2O$: the X = Fe- Mg-Mn-Zn compositional tetrahedron

PAOLO BALLIRANO*

Dipartimento di Scienze della Terra, Università di Roma "La Sapienza", P.le A. Moro 5, I-00185 Roma, Italy

Abstract: The paper is devoted to the investigation of the crystal chemistry of the halotrichite group $X Al_2(SO_4)_4 \cdot 22H_2O$ along the joints of the X = Fe-Mg-Mn-Zn compositional tetrahedron by means of X-ray powder diffraction and the Rietveld method on synthetic samples. Complete solid solution along the joints has been observed. The volume *vs*. $< r_x >$ plot (mean ionic radius of the X cation) indicate fairly large departures from the expected linearity. The reason/s of the departure from linearity is, at present, not clearly understood and could be possibly related to the combined effect of the different degree of filling of the *d* shell of the transition elements, the corresponding attraction/repulsion with the five facing lone pairs of the water molecules pertaining to the $XO(H_2O)_5$ octahedron, and to the different degree of ionicity of the X-O bond.

Key-words: sulfates, halotrichite-group, crystal chemistry, X-ray powder diffraction, Rietveld method.

Introduction

The halotrichite group consists of monoclinic hydrated sulfates, crystallizing in space group $P2_1/c$, whose general formula is $XY_2(SO_4)_4 \cdot 22H_2O$ where X is a divalent (Co^{2+}, Fe^{2+}, Mg^{2+}, Mn^{2+}, Ni^{2+}, and Zn^{2+}) and Y a trivalent (Al^{3+}, Cr^{3+}, and Fe^{3+}) cation (see Table 1 in Ballirano *et al*., 2003). According to the reported large isomorphic substitutions, complete solid solutions are expected to exist among the various end members. At the present structural data are available for apjohnite (XY_2 = $MnAl_2$, single-crystal data: Menchetti & Sabelli, 1976), halotrichite (XY_2 = $FeAl_2$, powder diffraction data: Lovas, 1986; Mihajlović *et al.*, 2002), pickeringite (XY_2 = $MgAl_2$, powder diffraction data: Quartieri *et al*., 2000), and dietrichite (XY_2 = $ZnAl_2$, powder diffraction data: Ballirano *et al*., 2003). As indicated by Ballirano *et al*. (2003), on the basis of a limited number of samples, a fairly linear trend between volume and mean ionic radius $< r_x >$ (Shannon, 1976) of the X cation is experimentally observed with an agreement index $R^2 = 0.907$. Small deviations from the trend seem to be, however, present. An accurate crystal chemical characterization of the group has been prevented, so far, by the impossibility to obtain pure natural samples of halotrichite-group minerals because of the small dimension of the crystals (generally sub-millimetric acicular crystals with very small shape factor, expressed as the ratio between width (W) and length (L), W/L; W *ca*. 0.5 μm) and by the occurrence of very complex mixtures with other sulfates (gypsum, epsomite *etc*.). Because of this, chemical analyses reported in reference data are often to be considered with caution. The aim of this paper is to carry out a systematic investigation of the crystal chemistry of the halotrichite group $X Al_2(SO_4)_4 \cdot 22H_2O$ along the joints of the X = Fe-Mg-Mn-Zn compositional tetrahedron by means of X-ray powder diffraction and the Rietveld method on synthetic samples.

Experimental methods

Synthesis

The various halotrichite-group terms were all prepared by dissolution of almost exact equimolar amounts of reagent grade $Al_2(SO_4)_3 \cdot 17H_2O$ (alunogen) and $X(SO_4) \cdot nH_2O$ (X = Fe-Mg-Mn-Zn) in distilled water and ensuing a complete slow evaporation of the solvent H_2O at room temperature. A small excess of alunogen was required to obtain the full combination of the salts. Due to the general strong tendency to adsorb water, the starting sulfate salts were kept for a week in an electric oven at 40°C before weighting. A total of 22 samples, with composition varying regularly at 25% steps, were synthesized (Table 1). Two further samples with composition $Mn_{85}Fe_{15}$ and $Mn_{35}Fe_{65}$ were also synthesized in order to have a more uniform

*E-mail: paolo.ballirano@uniroma1.it

DOI: 10.1127/0935-1221/2006/0018-0463

0935-1221/06/0018-0463 $ 3.15

distribution of terms within the investigated $< r_x >$ range. The resulting products consist of very thin acicular crystals (W/L < 0.05) in sub-parallel association similar to that reported by Ballirano *et al*. (2003) for dietrichite. Iron-containing terms are characterized by a color degrading from yellow (halotrichite *s.s.*) to yellowish-white. The remaining synthesized terms are white. Samples containing relevant amounts of Mn became pinkish after X-ray irradiation.

X-ray powder diffraction

X-ray powder diffraction data were collected on a parallel-beam automated diffractometer Siemens D5005, operating in transmission geometry, using Cu$K\alpha$ radiation. Each sample, prepared as capillary, was mounted and aligned on a standard goniometer head. The powders were loaded inside 0.5 or 0.7 mm diameter borosilicate glass capillaries, in order to analyze samples characterized by similar effective absorption $A_B = \mu R/\lambda$, hypothesizing a constant packing efficiency. Effective absorption measurements have been carried out collecting the transmitted beam through the samples $I_t(E)$ and the incident primary beam $I_0(E)$, both in direct transmission. The measured effective absorption was kept fixed throughout the refinement. Experimental details are reported in Table 2. Rietveld refinements were carried out by the GSAS crystallographic suite of programs (Larson & Von Dreele, 1985). Starting positional and displacement parameters were those of Ballirano *et al*. (2003) for dietrichite. The geometry of the system (89 atoms in the asymmetric unit) was restrained, similarly to Lovas (1986), Quartieri *et al*., (2000), Mihajlović *et al.* (2002), and Ballirano *et al.* (2003) using the following conditions: S^{IV}-O = 1.473(10) Å, O-S-O x 6 = 109.44(80)°, Al^{VI}-H_2O = 1.875(10) Å, H_2O-Al-H_2O x 12 = 90(1)°, H_2O-Al-H_2O x 3 = 180(1)°, H_2O(O)-M^{2+}-H_2O x 12 = 90(3)°, H_2O(O)-M^{2+}-H_2O x 3 = 180(3)°, O-H = 0.98(2) Å, H-O-H = 105(5)°. The values to be used as restrained distances $[X]^{VI}$-H_2O(O) were calculated in order to provide 2 formal charges to the divalent cation from bond-valence analysis (Breese & O'Keefe, 1991). The resulting values were Mg-O = 2.100(35) Å, Zn-O = 2.110(35) Å, Fe-O = 2.140(35) Å, Mn-O = 2.200(35) Å. Moreover the same bimodal hydrogen-bond network reported by Menchetti & Sabelli (1976) for apjohnite was used with O…H-O contact distances restrained to 1.74(14) and 2.14(14) Å, as previously done by Ballirano *et al.* (2003) for dietrichite. The total number of restraints was therefore of 213, 122 bonds and 91 angles. The statistical weight associated to each observation in each data set was selected in the 1.3-2 range, according to the fact that R_{exp} ($R_{exp} = wRp/\sqrt{\chi^2}$) was not constant for the various patterns. The contribution of the restraints to χ^2 was never exceeding 3.5%. The asymmetry-modified pseudo-Voigt of Finger *et al*. (1994) was chosen as peak profile function. Refined variables were GU ($\tan^2\theta$-dependent), GV ($\tan\theta$-dependent), and GW (angle-independent) Gaussian, LX ($(\cos\theta)^{-1}$-dependent) and LY ($\tan\theta$-dependent) Lorentzian and S/L, and H/L asymmetry parameters. The background was fitted with 36-terms Chebyshev polynomials of the first kind. Such a large number of terms was required to properly model the amorphous contribution of the capillary. Cell parameters, positional, and displacement parameters (for groups of equal atoms) were subsequently refined. U_{iso} displacement parameters for hydrogen atoms were kept fixed to 0.05 Å^2. Peak position was corrected for sample displacement from the focusing circle. The presence of preferred orientation was checked by means of the generalized spherical harmonics description of Von Dreele (1997). Small improvements of the fits were obtained as a result of texture indices in the 1.002 < J < 1.022 range. Small J values are consistent with the absence of preferred orientation, as expected for a capillary mount (J = 1: random sample; J = ∞: oriented single-crystal). Minor

Table 1. List of the synthesized samples.

Sample	Composition	Name
Fe_{100}	$FeAl_2(SO_4)_4 \cdot 22H_2O$	Halotrichite *s.s.*
$Fe_{75}Mg_{25}$	$(Fe_{0.75}Mg_{0.25})Al_2(SO_4)_4 \cdot 22H_2O$	
$Fe_{50}Mg_{50}$	$(Fe_{0.50}Mg_{0.50})Al_2(SO_4)_4 \cdot 22H_2O$	
$Fe_{25}Mg_{75}$	$(Fe_{0.25}Mg_{0.75})Al_2(SO_4)_4 \cdot 22H_2O$	
Mg_{100}	$MgAl_2(SO_4)_4 \cdot 22H_2O$	Pickeringite *s.s.*
$Mg_{75}Mn_{25}$	$(Mg_{0.75}Mn_{0.25})Al_2(SO_4)_4 \cdot 22H_2O$	
$Mg_{50}Mn_{50}$	$(Mg_{0.50}Mn_{0.50})Al_2(SO_4)_4 \cdot 22H_2O$	
$Mg_{25}Mn_{75}$	$(Mg_{0.25}Mn_{0.75})Al_2(SO_4)_4 \cdot 22H_2O$	
Mn_{100}	$MnAl_2(SO_4)_4 \cdot 22H_2O$	Apjohnite *s.s.*
$Mn_{85}Fe_{15}$	$(Mn_{0.85}Fe_{0.15})Al_2(SO_4)_4 \cdot 22H_2O$	
$Mn_{75}Fe_{25}$	$(Mn_{0.75}Fe_{0.25})Al_2(SO_4)_4 \cdot 22H_2O$	
$Mn_{50}Fe_{50}$	$(Mn_{0.50}Fe_{0.50})Al_2(SO_4)_4 \cdot 22H_2O$	
$Mn_{35}Fe_{65}$	$(Mn_{0.35}Fe_{0.65})Al_2(SO_4)_4 \cdot 22H_2O$	
$Mn_{25}Fe_{75}$	$(Mn_{0.25}Fe_{0.75})Al_2(SO_4)_4 \cdot 22H_2O$	
Zn_{100}	$ZnAl_2(SO_4)_4 \cdot 22H_2O$	Dietrichite *s.s.*
$Zn_{75}Fe_{25}$	$(Zn_{0.75}Fe_{0.25})Al_2(SO_4)_4 \cdot 22H_2O$	
$Zn_{50}Fe_{50}$	$(Zn_{0.50}Fe_{0.50})Al_2(SO_4)_4 \cdot 22H_2O$	
$Zn_{25}Fe_{75}$	$(Zn_{0.25}Fe_{0.75})Al_2(SO_4)_4 \cdot 22H_2O$	
$Zn_{75}Mg_{25}$	$(Zn_{0.75}Mg_{0.25})Al_2(SO_4)_4 \cdot 22H_2O$	
$Zn_{50}Mg_{50}$	$(Zn_{0.50}Mg_{0.50})Al_2(SO_4)_4 \cdot 22H_2O$	
$Zn_{25}Mg_{75}$	$(Zn_{0.25}Mg_{0.75})Al_2(SO_4)_4 \cdot 22H_2O$	
$Zn_{75}Mn_{25}$	$(Zn_{0.75}Mn_{0.25})Al_2(SO_4)_4 \cdot 22H_2O$	
$Zn_{50}Mn_{50}$	$(Zn_{0.50}Mn_{0.50})Al_2(SO_4)_4 \cdot 22H_2O$	
$Zn_{25}Mn_{75}$	$(Zn_{0.25}Mn_{0.75})Al_2(SO_4)_4 \cdot 22H_2O$	

Table 2. Experimental details of X-ray powder diffraction data collection.

Instrument	Siemens D5005
X-ray tube	Cu at 40 kV and 40 mA ($CuK\alpha_1$ = 1.540598 Å)
Incident beam optic	Multilayer X-ray mirrors
Sample mount	Rotating capillary (30 rpm)
Soller slits	2 (2.3° divergence)
Divergence and antidivergence slits	1 mm
Detector slit	0.2 mm (0.10°)
Detector	Solid state detector
2θ range (°)	4-110 (5301 data points)
Step size (°)	0.02
Counting time (s)	30

amounts of alunogen have been consistently detected in the diffraction pattern, as expected from the synthesis procedure (see above). Moreover a maximum amount of 2 wt% of $X(SO_4) \cdot nH_2O$ (X = Fe-Mg-Mn-Zn) was observed in a few samples indicating the almost perfect completeness of the crystallization. These sulfates were added to the refinement whenever occurring. Only cell parameters and weight fractions of the extra phases were refined. In order to reduce correlation among parameters the peak shape of the various phases was constrained to be equal. The absence of compositional inhomogeneities for each halotrichite sample was checked by evaluation of the peak broadening that was found substantially identical in all samples. Furthermore, the absence of compositional inhomogeneities may be confirmed by the substantially constant *esd* of the cell parameters of the various samples (see below). Miscellaneous data of refinements, cell parameters and relevant bond distances are reported in Table 3 and a selection of experimental, calculated, and difference plots in Fig. 1.

Table 3. Miscellaneous data of the refinements, cell parameters, and relevant bond distances. Statistical indicators as defined in Young (1993).

	Mg_{100}	$Mg_{75}Mn_{25}$	$Mg_{50}Mn_{50}$	$Mg_{25}Mn_{75}$	Mn_{100}	$Mn_{85}Fe_{15}$	$Mn_{75}Fe_{25}$	$Mn_{50}Fe_{50}$	$Mn_{35}Fe_{65}$
Rp	3.33	3.37	3.96	4.63	4.16	4.83	4.82	5.04	3.63
wRp	4.35	4.41	5.20	6.02	5.43	6.39	6.35	6.46	4.76
χ^2	1.225	1.211	1.099	1.051	1.161	1.065	1.033	1.107	1.064
Restr. contr. to χ^2 (%)	3.36	3.36	2.50	1.81	3.03	1.80	1.65	1.97	1.85
J	1.015	1.005	1.005	1.003	1.012	1.002	1.005	1.006	1.005
a(Å)	6.1793(2)	6.1852(1)	6.1886(2)	6.1924(2)	6.1998(2)	6.1996(2)	6.1982(3)	6.1946(5)	6.1953(2)
b(Å)	24.2540(9)	24.2851(6)	24.3047(7)	24.3286(9)	24.3590(7)	24.3461(10)	24.3381(11)	24.3122(18)	24.3024(7)
c(Å)	21.2055(9)	21.2283(5)	21.2416(6)	21.2592(8)	21.2861(7)	21.2833(9)	21.2806(10)	21.2709(17)	21.2648(9)
β(°)	100.344(2)	100.319(2)	100.289(2)	100.258(2)	100.228(2)	100.228(3)	100.225(3)	100.238(5)	100.246(2)
V(Å^3)	3126.5(3)	3137.1(2)	3143.6(2)	3151.6(2)	3163.6(2)	3161.4(3)	3159.3(3)	3152.5(5)	3151.3(2)
X-O(16) (Å)	2.041(16)	2.053(13)	2.085(13)	2.106(14)	2.124(14)	2.109(18)	2.100(16)	2.102(16)	2.111(14)
X-W(1) (Å)	2.094(19)	2.105(17)	2.158(18)	2.176(19)	2.241(19)	2.21(2)	2.19(2)	2.17(2)	2.164(18)
X-W(2) (Å)	2.104(18)	2.172(16)	2.167(16)	2.188(18)	2.217(18)	2.22(2)	2.20(2)	2.19(2)	2.183(17)
X-W(3) (Å)	2.067(18)	2.095(16)	2.143(17)	2.166(19)	2.183(17)	2.19(2)	2.18(2)	2.16(2)	2.153(18)
X-W(4) (Å)	2.070(19)	2.084(17)	2.107(18)	2.144(19)	2.157(19)	2.17(2)	2.167(19)	2.14(2)	2.133(18)
X-W(5) (Å)	2.076(18)	2.079(16)	2.100(17)	2.098(19)	2.161(18)	2.16(2)	2.14(2)	2.109(19)	2.130(17)
<X-O> (Å)	2.07(2)	2.10(4)	2.13(3)	2.15(3)	2.18(4)	2.18(4)	2.17(4)	2.14(3)	2.15(3)
$< r_x >$ (Shannon, 1976)	0.7200	0.7475	0.7750	0.8025	0.8300	0.8225	0.8175	0.8050	0.7975
<Al(1)-O> (Å)	1.877(4)	1.876(4)	1.876(4)	1.875(4)	1.879(3)	1.874(3)	1.875(3)	1.875(5)	1.875(3)
<Al(2)-O> (Å)	1.876(4)	1.875(3)	1.878(4)	1.875(2)	1.877(5)	1.878(3)	1.876(4)	1.873(4)	1.877(3)
<S(1)-O> (Å)	1.471(3)	1.471(5)	1.471(3)	1.474(2)	1.473(5)	1.474(6)	1.477(2)	1.477(4)	1.473(3)
<S(2)-O> (Å)	1.471(2)	1.468(5)	1.469(4)	1.470(1)	1.466(4)	1.469(3)	1.471(2)	1.471(2)	1.470(1)
<S(3)-O> (Å)	1.469(6)	1.469(0)	1.471(4)	1.470(2)	1.474(6)	1.472(2)	1.469(4)	1.471(2)	1.473(2)
<S(4)-O> (Å)	1.472(3)	1.474(4)	1.471(3)	1.473(2)	1.469(1)	1.472(2)	1.470(3)	1.472(1)	1.472(1)
	$Mn_{25}Fe_{75}$	Fe_{100}	$Fe_{75}Zn_{25}$	$Fe_{50}Zn_{50}$	$Fe_{25}Zn_{75}$	Zn_{100}	$Zn_{75}Mn_{25}$	$Zn_{50}Mn_{50}$	$Zn_{25}Mn_{75}$
Rp	4.38	3.65	3.78	3.81	3.54	3.72	3.58	4.24	4.68
wRp	5.73	4.81	5.05	5.06	4.67	4.85	4.72	5.53	6.12
χ^2	1.146	1.127	1.098	1.089	1.154	1.158	1.131	1.091	1.124
Restr. contr. to χ^2 (%)	2.32	2.34	2.24	2.11	2.64	2.77	2.55	2.28	1.83
J	1.005	1.004	1.006	1.007	1.007	1.005	1.006	1.009	1.003
a(Å)	6.1927(2)	6.1922(1)	6.1886(1)	6.1850(1)	6.1804(1)	6.1756(1)	6.1825(2)	6.1871(2)	6.1927(2)
b(Å)	24.2861(10)	24.2696(6)	24.2663(5)	24.2637(5)	24.2623(6)	24.2595(6)	24.2893(7)	24.3072(8)	24.3285(8)
c(Å)	21.2630(9)	21.2596(5)	21.2430(5)	21.2299(4)	21.2162(5)	21.1959(5)	21.2239(6)	21.2390(7)	21.2578(7)
β(°)	100.247(2)	100.260(2)	100.318(1)	100.362(1)	100.407(2)	100.454(2)	100.409(2)	100.352(2)	100.297(2)
V(Å^3)	3146.8(3)	3143.8(2)	3138.6(1)	3134.0(1)	3129.0(2)	3123.6(2)	3134.7(2)	3142.2(2)	3151.1(2)
X-O(16)	2.104(15)	2.060(13)	2.082(12)	2.077(13)	2.063(12)	2.063(12)	2.076(13)	2.090(13)	2.103(14)
X-W(1)	2.17(2)	2.149(18)	2.140(18)	2.127(15)	2.148(16)	2.100(15)	2.163(19)	2.153(17)	2.193(19)
X-W(2)	2.160(19)	2.179(16)	2.161(16)	2.180(16)	2.163(16)	2.146(15)	2.170(18)	2.194(18)	2.179(18)
X-:W(3)	2.15(2)	2.138(17)	2.143(16)	2.125(16)	2.097(16)	2.092(16)	2.136(18)	2.160(17)	2.162(18)
X-W(4)	2.12(2)	2.115(17)	2.103(18)	2.097(18)	2.071(18)	2.039(17)	2.086(19)	2.117(19)	2.14(2)
X-W(5)	2.108(19)	2.080(16)	2.080(17)	2.085(17)	2.083(16)	2.056(14)	2.078(17)	2.113(18)	2.140(18)
<X-O>	2.14(3)	2.12(4)	2.12(3)	2.11(3)	2.10(4)	2.08(3)	2.12(4)	2.14(3)	2.15(3)
$< r_x >$ (Shannon, 1976)	0.7925	0.7800	0.7700	0.7600	0.7500	0.7400	0.7625	0.7850	0.8075
<Al(1)-O> (Å)	1.875(6)	1.876(2)	1.874(3)	1.875(5)	1.877(5)	1.873(5)	1.874(1)	1.874(2)	1.873(4)
<Al(2)-O> (Å)	1.874(2)	1.875(2)	1.876(3)	1.875(3)	1.876(4)	1.877(4)	1.875(4)	1.873(2)	1.875(4)
<S(1)-O> (Å)	1.472(4)	1.475(4)	1.474(4)	1.468(7)	1.471(3)	1.470(4)	1.474(3)	1.472(6)	1.473(4)
<S(2)-O> (Å)	1.467(2)	1.471(3)	1.471(6)	1.469(3)	1.466(4)	1.466(4)	1.468(3)	1.468(2)	1.470(1)
<S(3)-O> (Å)	1.471(3)	1.474(2)	1.475(2)	1.472(3)	1.472(2)	1.471(3)	1.469(2)	1.470(2)	1.473(3)
<S(4)-O> (Å)	1.475(3)	1.473(5)	1.470(3)	1.472(1)	1.473(2)	1.470(2)	1.472(3)	1.470(4)	1.471(4)

to be continued p466

Table 3. (continued)

	$Mg_{75}Fe_{25}$	$Mg_{50}Fe_{50}$	$Mg_{25}Fe_{75}$	$Mg_{75}Zn_{25}$	$Mg_{50}Zn_{50}$	$Mg_{25}Zn_{75}$
Rp	3.44	3.50	4.34	4.24	3.86	3.39
wRp	4.53	4.62	5.70	5.59	5.21	4.49
χ^2	1.137	1.113	1.054	1.096	1.114	1.117
Restr. contr. to χ^2 (%)	2.69	2.47	1.35	2.54	2.10	2.66
J	1.006	1.002	1.002	1.006	1.011	1.022
a(Å)	6.1847(1)	6.1876 (1)	6.1909(3)	6.1786(2)	6.1777(1)	6.1764(1)
b(Å)	24.2549(6)	24.2590(5)	24.2640(11)	24.2572(7)	24.2604(6)	24.2583(5)
c(Å)	21.2297(5)	21.2414(5)	21.2595(10)	21.2012(6)	21.2021(5)	21.1968(5)
β(°)	100.322(1)	100.308(1)	100.274(3)	100.378(2)	100.401(2)	100.415(1)
V(Å^3)	3133.1(2)	3137.0(1)	3142.3(3)	3125.6(2)	3125.4(2)	3124.7(1)
X-O(16) (Å)	2.046(13)	2.050(12)	2.080(17)	2.031(13)	2.050(13)	2.061(11)
X-W(1) (Å)	2.102(15)	2.114(15)	2.13(2)	2.086(17)	2.095(16)	2.106(15)
X-W(2) (Å)	2.143(15)	2.150(14)	2.14(2)	2.133(16)	2.155(17)	2.160(15)
X-W(3) (Å)	2.109(15)	2.114(14)	2.11(2)	2.099(17)	2.117(17)	2.115(16)
X-W(4) (Å)	2.068(16)	2.088(15)	2.11(2)	2.055(18)	2.079(18)	2.051(16)
X-W(5) (Å)	2.070(16)	2.077(16)	2.09(2)	2.036(17)	2.046(17)	2.063(15)
<X-O> (Å)	2.09(3)	2.10(3)	2.11(2)	2.07(4)	2.09(4)	2.09(4)
$< r_x >$ (Shannon, 1976)	0.7350	0.7500	0.7650	0.7250	0.7300	0.7350
<Al(1)-O> (Å)	1.876(5)	1.876(5)	1.875(2)	1.875(5)	1.876(4)	1.874(5)
<Al(2)-O> (Å)	1.876(3)	1.876(2)	1.876(2)	1.876(4)	1.877(3)	1.874(5)
<S(1)-O> (Å)	1.472(3)	1.472(5)	1.473(3)	1.472(3)	1.470(4)	1.472(4)
<S(2)-O> (Å)	1.468(2)	1.467(5)	1.470(2)	1.467(1)	1.469(4)	1.470(6)
<S(3)-O> (Å)	1.472(3)	1.476(3)	1.471(1)	1.469(1)	1.469(3)	1.471(2)
<S(4)-O> (Å)	1.473(3)	1.473(5)	1.474(2)	1.473(2)	1.470(1)	1.471(3)

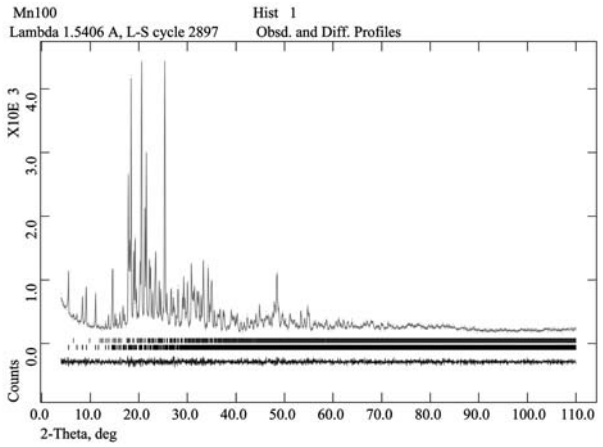

a)

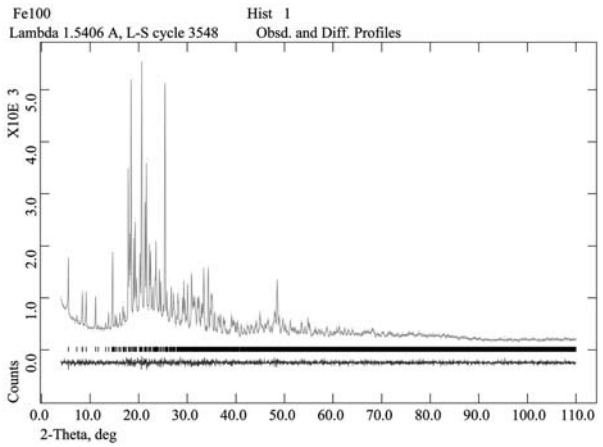

b)

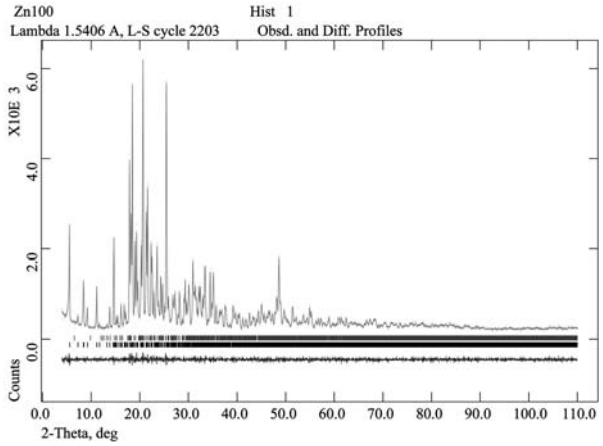

c)

Fig. 1. Experimental (dots) and calculated (continuous line) Rietveld plots for a) $MnAl_2(SO_4)_4 \cdot 22H_2O$ (apjohnite), b) $FeAl_2(SO_4)_4 \cdot 22H_2O$ (halotrichite), c) $ZnAl_2(SO_4)_4 \cdot 22H_2O$ (dietrichite). The difference profile is shown at the bottom of the figure. Vertical markers refer to the positions of the calculated Bragg reflections. In the case of apjohnite and dietrichite the upper line indicate Bragg reflections of alunogen and the lower line those of the halotrichite-group mineral.

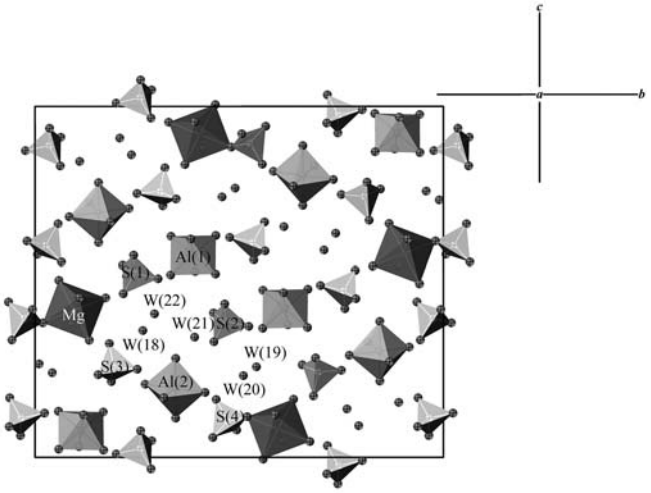

Fig. 2. Drawing of the structure of $MgAl_2(SO_4)_4 \cdot 22H_2O$ (pickeringite) projected along [100].

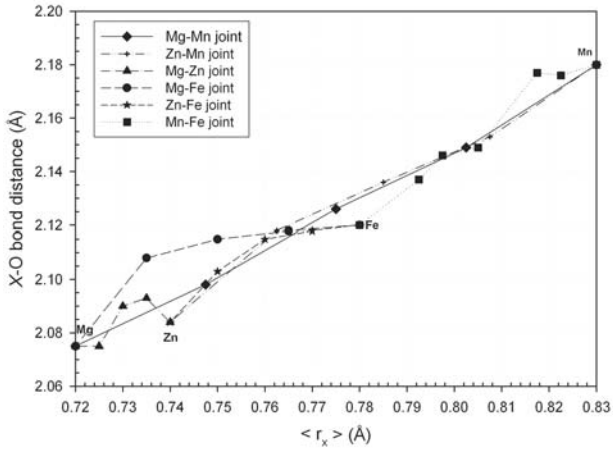

Fig. 3. Plot of mean $[X]^{VI}$-H_2O(O) bond distances *vs* mean ionic radius $< r_x >$ of the *X* cation.

Discussion

Structure description

A complete solid solution along the joints of the *X* = Fe-Mg-Mn-Zn Y = Al compositional tetrahedron has been observed. Rietveld refinements have confirmed, as expected, that the various terms of the family are isostructural. Each asymmetric unit contains one $XO(H_2O)_5$ octahedron, two independent $Al(H_2O)_6$ octahedra (Al(1) and Al(2)), and four independent SO_4 tetrahedra (S(1), S(2), S(3), and S(4)). The $XO(H_2O)_5$ octahedron and the S(4)-centered tetrahedron are linked *via* O(16) thus forming a neutral $[X(SO_4)(H_2O)_5]^0$ cluster (Hawthorne *et al.*, 2000). This cluster is also found in quenstedtite $[Fe^{3+}(H_2O)_4(SO_4)_2)][Fe^{3+}(H_2O)_5(SO_4)](H_2O)_2$ (Thomas *et al*., 1974). Of the 22 water molecules per asymmetric unit, 17 are co-ordinated with one *X* and two Al cations, whereas the remaining five are linked solely *via* weak hydrogen bonds to oxygen atoms of the sulfate group or further H_2O molecules. The $[X(SO_4)(H_2O)_5]^0$ cluster, the $Al(H_2O)_6$ octahedra, and the remaining SO_4 tetrahedra are arranged in such a way to form hexagonal channels, running along [100] (Fig. 2). It is also worth noticing that the $[X(SO_4)(H_2O)_5]^0$ cluster represents the "extra content" of any halotrichite-group mineral with respect to alunogen, one of the starting salts. Alunogen structure consists of double sheets made up of two $Al(H_2O)_6$ octahedra and two SO_4 tetrahedra running along [010]. The remaining SO_4 tetrahedron is located between adjacent double sheets. Moreover, similarly to halotrichite-group minerals, the structure shows hexagonal channels but in this case built up by three $Al(H_2O)_6$ octahedra and three SO_4 tetrahedra running along [100] (Menchetti & Sabelli, 1974). Mean bond distances within $Al(H_2O)_6$ octahedra and SO_4 tetrahedra are extremely constant and no significant trend has been observed within the halotrichite-group minerals (Table 3). Moreover they are very similar to those reported by Menchetti & Sabelli (1974, 1976) for both alunogen and apjohnite. Structural data confirm a substantial linearity between mean $[X]^{VI}$-H_2O(O) bond distances and mean ionic radius of the cation occupying the *X* position (Fig. 3). As a general remark, the refined mean $[X]^{VI}$-H_2O(O) bond distances are somewhat shorter than the corresponding restrained values resulting in a small overbonding of the *X* cation (less that 7% of the expected 2 formal charges). Moreover, the *X*-O(16) is consistently shorter and the *X*-W(1) and *X*-W(2) larger than the remaining bond distances. This is in substantial agreement with data of Menchetti & Sabelli (1976) and Ballirano *et al.* (2003) but in disagreement with those of Quartieri *et al*. (2000). The shortening of the *X*-O bond distance is also observed in quenstedtite (Thomas *et al*., 1974). Moreover the bond distances reported in Menchetti & Sabelli (1974) for an apjohnite of approximate composition $X = Mn_{0.66}Mg_{0.34}$ are in good agreement with the reported trend within the Mn-Mg joint (see Table 3). The same does not apply to the pickeringite sample of Quartieri *et al*. (2000) whose mean $[X]^{VI}$-H_2O(O) bond distance of 2.009(20) Å is significantly shorter than expected showing a strong overbonding at *X* (2.517 formal charges from bond-valence analysis considering the site as fully occupied by Mg).

Cell parameters vs. mean ionic radius behaviour within the group

Plots of volume, *a*, *b*, *c*, and β *vs.* mean ionic radius $< r_x >$ of the *X* cation are reported in Fig. 4 to 8. The volume *vs.* $< r_x >$ plot (Fig. 4) indicates fairly large departures from the expected, on the basis of a purely ionic model, linearity. Irregularities in such volume *vs.* $< r_x >$ plot may be also observed in Tutton's salts and $XSO_4 \cdot 6H_2O$ series (Ballirano *et al*. in prep.) both characterized by the presence of $[X]^{VI}$-H_2O polyhedra. However, in the case of halotrichites the irregularities take a different behaviour possibly related to the presence of $[X]^{VI}$-H_2O(O) instead of $[X]^{VI}$-H_2O polyhedra. The more striking departure from linearity is shown by the Zn-bearing terms that, as in the case of natural dietrichite (see Fig. 6 of Ballirano *et al*., 2003), are characterized by smaller volumes than expected

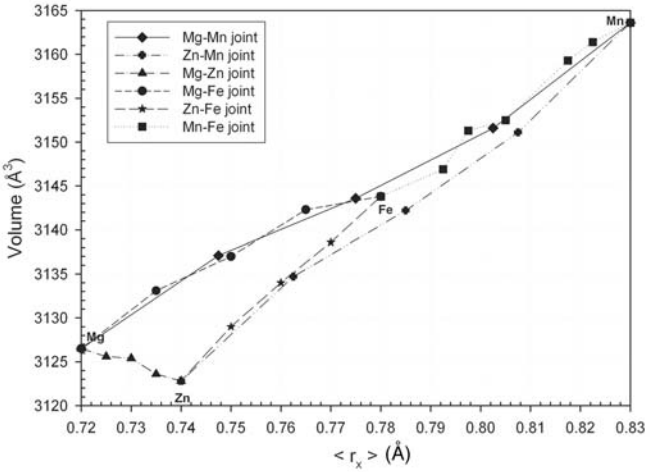

Fig. 4. Plot of volume *vs* mean ionic radius < r_x > of the *X* cation. Error bars smaller than symbols.

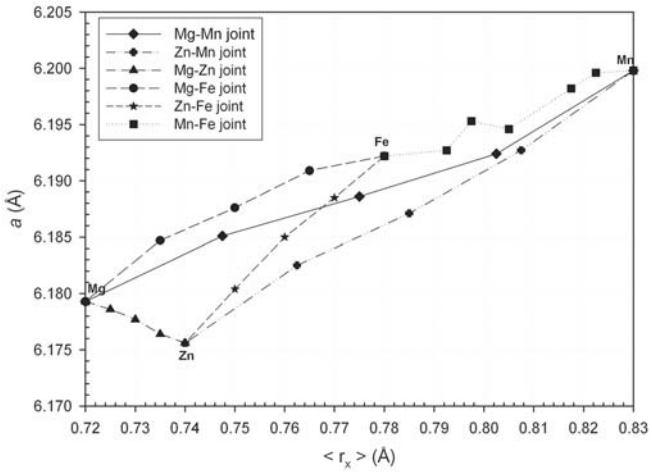

Fig. 5. Plot of *a vs* mean ionic radius < r_x > of the *X* cation. Error bars smaller than symbols.

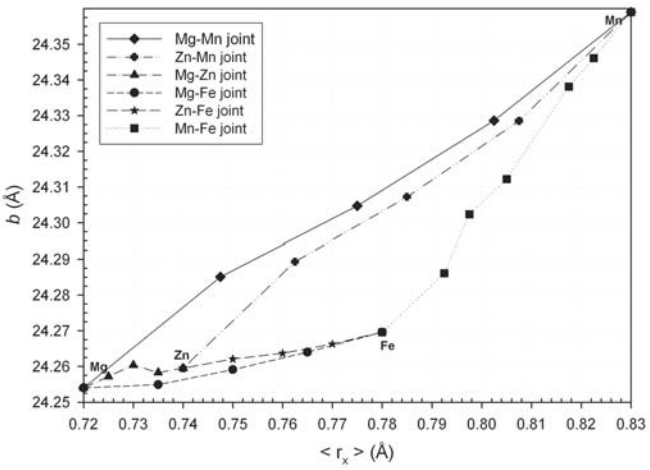

Fig. 6. Plot of *b vs* mean ionic radius < r_x > of the *X* cation. Error bars smaller than symbols.

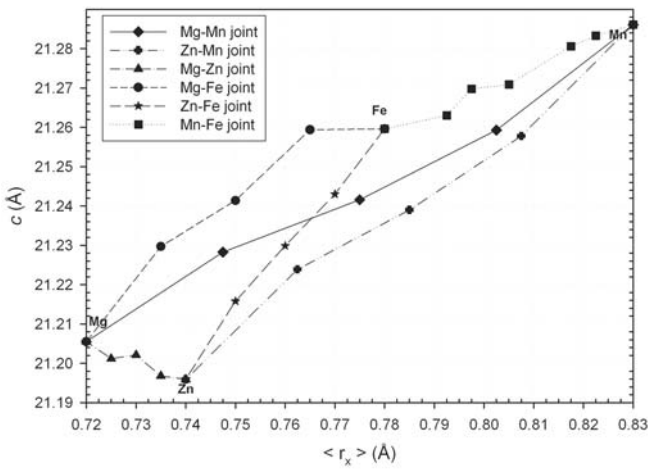

Fig. 7. Plot of *c vs* mean ionic radius < r_x > of the *X* cation. Error bars smaller than symbols.

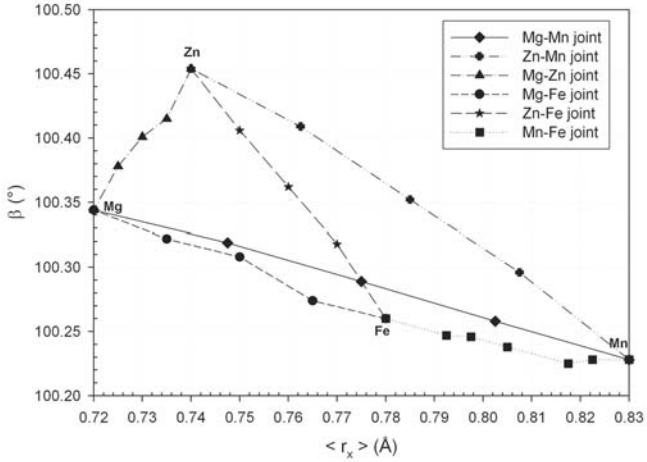

Fig. 8. Plot of β *vs* mean ionic radius < r_x > of the *X* cation. Error bars smaller than symbols.

on the basis of < r_x > as tabulated in Shannon (1976). The "Zn-contraction" occurs as the result of the decreasing of the *a* and *c* cell parameters (Fig. 5 and 7) whereas *b* (Fig. 6) and β (Fig. 8) both increase with respect to the expected trend. Also Fe-bearing terms seem to show some minor displacement from the expected trend. More in detail Mg, Zn, and Mn end-members define the vertices of a outer triangle (Fig. 4) with the Fe end-member located approximately at its centroid. Linearity seems to be substantially obeyed within each binary joint. The *a vs.* < r_x > (Fig. 5) and *c vs.* < r_x > (Fig. 7) plots have common features. In both cases Fe-bearing terms show cell parameters more expanded than expected from < r_x > whereas Zn-bearing terms show a marked contraction. The behaviour of the *b vs.* < r_x > and β *vs.* < r_x > plots is, on the contrary, quite different. In the case of the *b vs.* < r_x > plot the four end-members are located approximately along an arc (Fig. 6), the Zn end-member being slightly displaced toward the

focus. Zn-bearing terms are characterized by a markedly expanded β angle (Fig. 8). The reason/s of the departure from linearity observed within the volume *vs.* $< r_x >$ plot is, at present, not clearly understood and could be possibly related to the combined effect of the different degree of filling of the *d* shell of the transition elements (Fe d^5, Mn d^6, Zn d^{10}), the corresponding attraction/repulsion with the five facing lone pairs of the water molecules pertaining to the $XO(H_2O)_5$ octahedron, and to the different degree of ionicity of the *X*-O bond, spanning from *ca.* 68% for Mg-O to *ca.* 48% in the case of Fe-O (as calculated from Pauling's electronegativity). In particular both Fe (High Spin, HS) and Zn shows a spherical distribution of electrons with one (Fe HS) or two (Zn) electrons in each one of the five orbitals. A charge-density study could be possibly able to provide some insights about these irregularities.

Acknowledgements: Thanks are due to Mr. Paolo Ceccarelli for help in synthesis work. The author greatly appreciated the constructive review of the manuscript by Martin Kunz and an anonymous referee. This work has received financial support from Università di Roma "La Sapienza" and MIUR Cofin.

References

Ballirano, P., Bellatreccia, F., Grubessi, O. (2003): New crystal-chemical and structural data of dietrichite, ideally $ZnAl_2(SO_4)_4 \cdot 22H_2O$, a member of the halotrichite group. *Eur. J. Mineral.*, **15**, 1043-1049.

Breese, N.E. & O'Keefe, M. (1991): Bond-valence parameters for solids. *Acta Cryst.*, **B47**, 192-197.

Finger, L.W., Cox, D.E., Jephcoat, A.P. (1994): A correction for powder diffraction peak asymmetry due to axial divergence. *J. Appl. Cryst.*, **27**, 892-900.

Hawthorne, F.C., Krivovichev, S.V., Burns, P.C. (2000): The crystal chemistry of sulfate minerals. *in* "Sulfate Minerals – Crystallography, Geochemistry, and Environmental Significance", C.N. Alpers, J.L., Jambor, D.K. Nordstrom, eds. *Reviews in Mineralogy & Geochemistry*, Mineralogical Society of America, Washington pp. 1-112.

Larson, A.C. & Von Dreele, R.B. (1985): GSAS General Structure Analysis System. LAUR 86-748, Los Alamos National Laboratory. The Regents of the University of California.

Lovas, G.A. (1986): Structural study of halotrichite from Recsk (Matra Mts., N-Hungary). *Acta Geol. Hung.*, **29**, 389-398.

Menchetti, S. & Sabelli, C. (1974): Alunogen. Its structure and twinning. *Tschermaks Min. Petr. Mitt.*, **21**, 164-178.

—,— (1976): The halotrichite group: the crystal structure of apjohnite. *Min. Mag.*, **40**, 599-608.

Mihajlović, T., Karanović, L., Dimitrijević, R. (2002): The crystal structure of halotrichite ($FeAl_2(SO_4)_4 \cdot 22H_2O$) from the mercury mine Šuplja stena on Mt. Avala, Serbia. *Z. Kristallogr.*, Suppl. No. 19, 88.

Quartieri, S., Triscari, M., Viani, A. (2000): Crystal structure of the hydrated sulphate pickeringite ($MgAl_2(SO_4)_4 \cdot 22H_2O$): X-ray powder diffraction study. *Eur. J. Mineral.*, **12**, 1131-1138.

Shannon, R.D. (1976): Revised effective ionic radii and systematic studies of interatomic distances in halides and chalcogenides. *Acta Cryst.*, **A32**, 751-767.

Thomas, J.N., Robinson, P.D., Fang, J.H. (1974): Crystal structure and mineral chemistry of hydrated ferric sulfates: IV. The crystal structure of quenstedtite. *Am. Mineral.*, **59**, 582-586.

Von Dreele, R.B. (1997): Quantitative texture analysis by Rietveld refinement. *J. Appl. Cryst.*, **30**, 517-525.

Young, R.A. (1993): Introduction to the Rietveld method. *in* "The Rietveld method", R.A. Young, ed. Oxford Science, Oxford, pp. 1-38.

Received 7 September 2005
Modified version received 24 February 2006
Accepted 29 March 2006